Gigacycle fatigue behavior of austenitic stainless steels used for mercury target vessels

Takashi Naoe[a], Xiong Zhihong[b], Masatoshi Futakawa[a]

[a] *Japan Atomic Energy Agency, Tokai-mura, Naka-gun, Ibaraki 319-1195, Japan.*
[b] *Graduate School of Science and Engineering, Ibaraki University, Nakanarusawa, Hitachi, Ibaraki 316-8511, Japan*

Abstract

A mercury enclosure vessel for the pulsed spallation neutron source manufactured from a type 316L austenitic stainless steel, a so-called target vessel, suffers the cyclic loading caused by the proton beam induced pressure waves. A design criteria of the JSNS target vessel which is defined based on the irradiation damage is 2500 hours at 1 MW with a repetition rate of 25 Hz, that is, the target vessel suffers approximately 10^9 cyclic loading while in operation. Furthermore, strain rate of the beam window of the target vessel reaches 50 s^{-1} at the maximum, which is much higher than that of the conventional fatigue. Gigacycle fatigue strength up to 10^9 cycles for solution annealed 316L (SA) and cold-worked 316L (CW) were investigated through the ultrasonic fatigue tests. Fatigue tests were performed under room temperature and 250 °C which is the maximum temperature evaluated at the beam window in order to investigate the effect of temperature on fatigue strength of SA and CW 316L. The results showed that the fatigue strength at 250 °C is clearly reduced in comparison with room temperature, regardless of cold work level. In addition, residual strength and micro hardness of the fatigue tested spec-

Email address: naoe.takashi@jaea.go.jp (Takashi Naoe)

Preprint submitted to Journal of Nuclear Material (special issue on IWSMT-12) January 17, 2017

imen were measured to investigate the change in mechanical properties by cyclic loading. Cyclic hardening was observed in both the SA and CW 316L, and cyclic softening was observed in the initial stage of cyclic loading in CW 316L. Furthermore, abrupt temperature rising just before fatigue failure was observed regardless of testing conditions.

Keywords: Gigacycle fatigue, Pressure waves, High-strain rate, Cold work, Mercury, Cyclic hardening, Cyclic softening

1. Introduction

A liquid mercury target system providing pulsed neutron beams has been operating at the Japan Spallation Neutron Source (JSNS) in the Japan Proton Accelerator Research Complex (J-PARC) [1]. High-intense proton beams, up to 1 MW at 25 Hz with a 1 μs in a pulse duration, are injected into the liquid mercury to produce spallation neutrons. A mercury enclosure vessel made from type 316L stainless steel, a so-called target vessel is loaded with cyclic stresses resulting from the thermal energy and pressure waves induced by the proton beam bombardment [2]. The target vessel also suffers proton and neutron irradiation and the liquid mercury immersion. An original design criteria of the JSNS target vessel was decided temporary to below 5 dpa based on ductility under irradiation, which should remain acceptable for a lifetime of 2500 hours at 1 MW [3]. The target vessel, therefore, suffers approximately 10^9 cyclic loading during operation. Furthermore, the strain rate at the beam window of the target vessel reaches up to ca. 50 s^{-1} at the maximum, which is much higher than that of conventional fatigue loadings [4].

On the basis of the off-beam and on-beam damage experiments, cavitation

damage owing to pressure waves is the main factor to determine the service life of the target vessel rather than the irradiation damage at present [5]. The fatigue crack propagation originates readily at the cavitation damaged area. Reduction of the residual strength due to inclusions was observed in the target vessel of the Spallation Neutron Source at the Oak Ridge National Laboratory (ORNL) [6, 7]. In general, the gigacycle fatigue strength is reduced by inclusion. Therefore, the gigacycle fatigue will be an important factor influencing the lifetime of the target vessel.

In general, the fatigue failure in gigacycle experiments occurs earlier than that of the fatigue limit, based on the results of conventional fatigue tests up to 10^7 cycles. It is known that the internal failure originating from inclusions occurs in the gigacycle region for the high strength steels [8]. For austenitic stainless steels, it was reported that the internal failure was observed at higher than 10^7 cycles in the case of the pre-strained (cold-worked) material, whereas the fatigue failure originating from the surface was dominant in the case of the solution annealed material [9, 10].

On the other hand, Liquid Metal Embrittlement (LME), a phenomenon that occurs when solid metal is in contact with liquid metals, may affect the fatigue life in gigacycle. It was reported that the low cycle fatigue strength degradation with grain boundary failure of austenitic stainless steels by mercury immersion, and the effect seemed to be depending on the immersion time (testing frequency) [11, 12]. The authors previously investigated the fatigue crack propagation in mercury through the bending fatigue test [13]. The results showed that the crack growth rate was slightly accelerated by mercury. It was also reported the quasi-static elongation of austenitic stainless steel was degraded by mercury immersion, but

the degradation was dependent on strain rate [14].

Gigacycle fatigue strength for the solution annealed type 316L stainless steel (SA 316L) and the cold worked 316L (CW 316L) were investigated through an ultrasonic fatigue test in this study. Fatigue tests were conducted under room temperature and 250 °C, which is the maximum temperature evaluated at the beam window of the target vessel in order to investigate the effect of testing temperature on gigacycle fatigue strength under high-strain rate loading. Furthermore, the mechanical properties change due to the cyclic loading were investigated through the tensile test and micro-indentation test.

2. Experimental procedure

2.1. Material and specimen

Type 316L austenitic stainless steel, which is the structural material of the mercury target vessel, was selected for the gigacycle fatigue tests. Table 1 shows the chemical compositions of the material. The as-received plate of 15 mm thickness has been solution-annealed at 1120 °C for 7.5 min with a water quench (hereinafter referred to as SA 316L). A part of the SA 316L plate was cold-rolled to 10% and 20% reduction in thickness to increase the dislocation density to simulate irradiation hardened materials, hereinafter referred to as 10%CW and 20%CW, respectively. 20%CW material closely matches the mechanical properties of SA 316L steel irradiated to 1 dpa irradiation below 100 °C [11].

An hour-glass shape specimens were machined from the SA and CW 316L plates, and were used for the fatigue test as shown in Fig. 1. The longitudinal direction of the specimen was always made perpendicular to the direction of working, i.e. Transverse Direction (T.D.). The surface roughness of the specimen was

Table1. Chemical composition of type 316L stainless steel for the fatigue test

wt.%	Fe	Cr	Ni	Mo	Mn	C	Si	P	S
316L	Bal.	17.55	12.09	2.10	0.84	0.011	0.43	0.027	0.001

as-machined (Ra=0.46 μm, Rz=2.4 μm). It is well known that the surface roughness of a specimen has the effect on fatigue strength. In the previous study, the effect of surface finish on ultrasonic fatigue test was investigated by using the buff-polished and as-machined specimens [4]. The result showed that the as-machined surface had no effect on fatigue strength compared with the polished surface, and estimated $\sqrt{area}$ value, which is the square root of the projection area of defect [15], of as-machined specimen was smaller than that of the effective value on fatigue limit.

In order to investigate the effect of mercury on the gigacycle fatigue strength, fatigue test was conducted using the mercury immersed specimens. It is reported that the fatigue strength was obviously degraded under the condition of mercury immersion at room temperature [11–13]. However, it is difficult to conduct the ultrasonic fatigue testing under the condition of mercury immersion. Accordingly, the mercury immersed specimen was used for the fatigue test. A part of machined SA 316L specimens were immersed in mercury for 5000 hours at room temperature. After mercury immersion, the specimen was washed in ethanol with an ultrasonic bath to remove the mercury from the specimen surface and conduct the fatigue test.

2.2. Ultrasonic fatigue test

Load controlled gigacycle fatigue tests were conducted using an ultrasonic fatigue testing system (Shimadzu, USF-2000). Fig. 2 shows the photograph of the

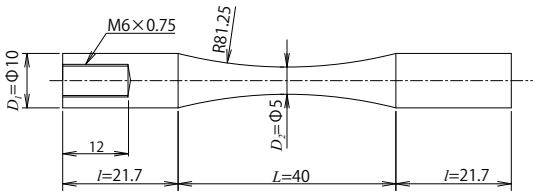

Fig. 1. Hour-glass shape fatigue test specimen. Dimensions in millimetres.

experimental setup. The ultrasonic oscillation was applied to one end of the specimen through the piezoelectric actuator of 20 kHz in resonance frequency. Ratio of stress $R = \sigma_{max}/\sigma_{min}$ in this experiment is -1, that is tensile–compression. The applied stress amplitude to the specimen, σ_a, was estimated from the following equations[16]:

$$\sigma_a = aE\beta \cos\left(\frac{\omega l}{c}\right) \cosh\left(\frac{bL}{2}\right) \left(\frac{1}{\frac{2}{L}\sinh\beta}\right), \tag{1}$$

$$b = \frac{2}{L} \cosh^{-1}\left(\frac{D_1}{D_2}\right), \tag{2}$$

$$\beta = \sqrt{b^2 - \left(\frac{\omega}{c}\right)^2}, \tag{3}$$

where a is the displacement amplitude of the specimen, E is the Young's modulus, c is the sound speed described as $\sqrt{E/\rho}$, ρ is the density, l and L are dimensions of the specimen shown in Fig. 1. The strain rate of the specimen which depending on the stress amplitude is approximately 10^2 s^{-1}.

The surface temperature of the specimen is rapidly increased due to the self-heating by ultrasonic oscillation, especially, since austenitic stainless steel has a low heat conductivity and a large internal friction. In order to control the specimen temperature during the ultrasonic fatigue test, intermittent loading and air cooling were applied in this experiment. The former is conducted by controlling the load-

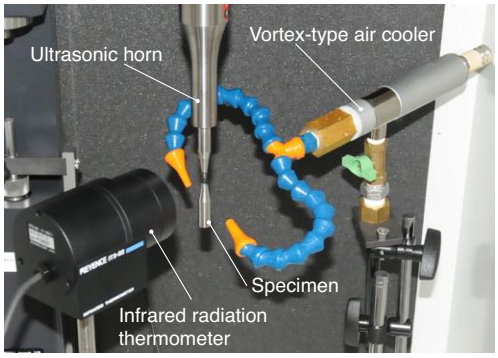

Fig. 2. Photograph of the experimental setup for the ultrasonic fatigue test.

ing and arresting interval of ultrasonic oscillation, the latter is done by blowing cold air on the specimen surface using the vortex-type air cooler. The surface temperature of the specimen was monitored using an infrared radiation thermometer (Keyence, IT2-02) in which spot diameter and sampling rate are 1.2 mm and 5 Hz, respectively. Fatigue tests in this experiment were conducted under the conditions of room temperature and 250 °C by controlling the flow rate of cooling air to investigate the effect of testing temperature on fatigue strength. Displacement of the specimen was calibrated in each material using an eddy current gage (Applied Electronics, PU-05). Fatigue failure of the specimen in this experiment was defined as the number of cycles at which the resonance frequency of the specimen exceeds by ±500 Hz the initial frequency due to the occurrence of the microcrack.

2.3. Mechanical properties measurement

After the ultrasonic fatigue tests, quasi-static tensile tests were performed to measure the ultimate tensile strength as the residual strength using the fatigue-tested specimen. The parallel part of the specimen was chucked and tensile stress was applied at the constant crosshead speed of 5 mm/min using a hydraulic test-

ing machine (Shimadzu, 4890-servolulser). Fracture surfaces of the tensile specimens were observed by using a scanning electron microscope (SEM, Keyence, VE-7800) and optical microscope (Keyence, VHX-900), in order to localize the fatigue crack origin due to cyclic loading.

Some parts of the fatigue-tested specimens without tensile test were cut in a longitudinal direction and buff-polished for microhardness measurement. Microhardness was measured using the microhardness tester (Shimadzu, DUH-W201S) with the Berkovich tip to investigate the change in the hardness by cyclic loading. The load–depth curve was continuously measured, and the universal hardness, H_u, was evaluated using the following equation;

$$H_u = \frac{L_{max}}{26.43 D_{max}}, \tag{4}$$

where L_{max} is the maximum load applied to the specimen and D_{max} is the maximum depth of indent [17]. The maximum load and loading rate were 29.4 mN and 1.47 mN/sec, respectively.

3. Results

3.1. Specimen temperature

A typical example of the measurement result for the displacement and the surface temperature of the specimen for 20%CW 316L at σ_a=435 MPa are shown in Fig. 3. Time of intermittent loading and arresting are 0.11 s and 5.0 s, respectively. It can be seen that the specimen is elongated approximately 5 μm after a period of oscillations due the thermal expansion. On the other hand, the temperature of the specimen surface, because the sampling rate of the thermometer is insufficient, seems to be delayed with the loading, and is gradually decreasing the arresting

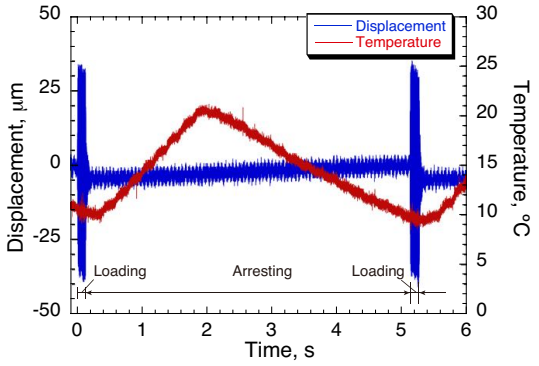

Fig. 3. Example of the displacement at the bottom side and surface temperature at the center of the specimen during the fatigue test for 20%CW 316L at σ_a=435 MPa.

time. Fig. 4 shows the change in the specimen surface temperature as a function of the number of cycles for SA 316L tested at room temperature (RT) and 250 °C (HT). In the case of HT, surface temperature was fluctuating because the flow rate of the cooling air was manually controlled to keep the surface temperature around 250 °C. It can be seen that the abrupt temperature rise just before failure are observed for both RT and HT. It was also recognized that the tempering color due to the temperature rise on the center part of the specimen surface was circular. It is noted that the temperature just before failure in the test at 250 °C is saturated due to thermometer overrange. The abrupt temperature rise was occurred after reaching approximately 99% of lifetime in this experiment.

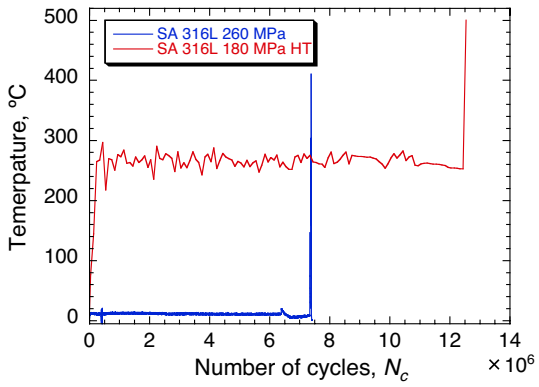

Fig. 4. Change in the specimen temperature as a function of the number of cycles for SA 316L tested at room temperature (RT) and 250 °C (HT).

3.2. Fatigue strength

3.2.1. Effect of cold work on fatigue strength

The S–N (the stress amplitude and the number of cycles to failure) curves for SA 316L, 10%CW, and 20%CW at room temperature, under high-strain rate obtained by the ultrasonic fatigue tests are summarized in Fig. 5. In order to compare with the conventional fatigue test, comparison fatigue data of the same SA 316L tested at 1 Hz under a stress ratio of 0.1, and reference SA316LN at 10 Hz [11], under a stress ratios of 0.1 and -1 and strain rate approximately 10^{-1} $s^{-}1$ are shown in Fig. 5. It can be seen that the SA 316L at 1 Hz with $R = 0.1$ close to the SA 316LN at 10 Hz and $R = 0.1$. On the other hand, fatigue strength of SA 316L at 20 kHz with $R = -1$ seems to be higher than that of SA 316LN at 10 Hz with $R = -1$. It is suggested that the fatigue strength under the high-strain rate is higher than that under normal strain rate.

It is also recognized that the fatigue failure occurred after a number of cycles

higher than 10^7 in the ultrasonic fatigue tests, and obviously the fatigue limit is not reached up to 10^9 cycles, regardless of the cold work level. Fatigue strength of 10%CW and 20%CW 316L are clearly higher than that of SA 316L because of increase of yield stress due to the work hardening. However, no obvious differences are observed between 10%CW and 20%CW in the region of high-cycles (from 10^4 to 10^7 cycles). To quantitatively compare the difference of fatigue strength due to the cold work level, the fatigue data are represented by the following S–N relations [18];

$$\sigma_a = a \log N_f + b, \tag{5}$$

where σ_a and N_f are the applied stress amplitude and the number of cycles to failure, respectively, and a and b are the fitting constants. Fitted results of each material are shown in Fig. 5. The fatigue degradation rate, which is defined as the slope of the fatigue curve, a, for SA, 10%CW, and 20%CW 316L are -23.4, -23.2, and -8.43, respectively, and decreases with the increase of in the cold work level. That is, the sensitivity of stress amplitude on fatigue life decreases with the cold work level.

3.2.2. Effect of testing temperature on fatigue strength

The S–N curves for SA and 10%CW 316L at room temperature (RT) and 250 °C (HT) are summarized in Fig. 6. It is noted that the stress amplitude at 250 °C are estimated with considering the reduction of the Young's modulus by temperature rise. It can be seen that the fatigue strengths under HT are clearly reduced in compared with RT regardless of the cold work level. The slope of a in Eq. (5) for SA and 10%CW 316L at HT are -10.7 and -30.6, respectively. The reduction of the fatigue strength by high-temperature, calculated as the normalized fatigue strength of HT at a given number of cycles normalized at RT,

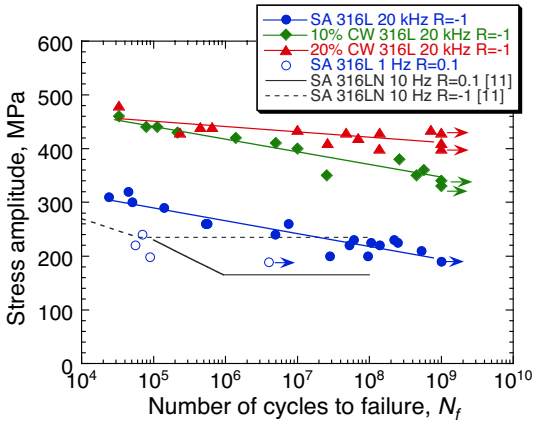

Fig. 5. S–N curves of SA, 10% CW, and 20% CW 316L for the ultrasonic fatigue test at room temperature. SA 316L 1Hz denotes the SA 316L tested at 1 Hz with R = 0.1 using the same material with the ultrasonic fatigue test. SA 316LN lines were cited from Reference [11].

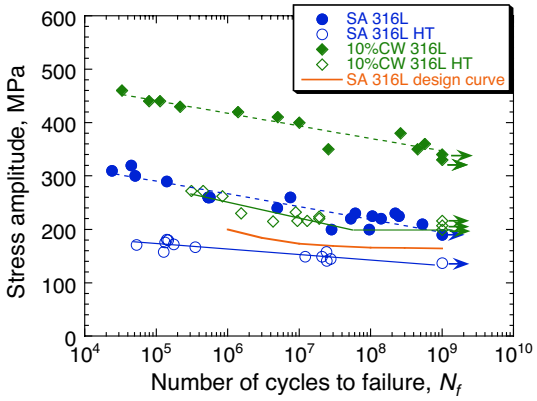

Fig. 6. S–N curves of SA316L and 10% CW tested at room temperature (RT) and 250 °C (HT).

approximately 0.61 for SA 316L, is slightly higher than that of 10%CW 316L, approximately 0.60. It is also reported that the fatigue strength in low cycle region and the fatigue limit is reduced by temperature rise under the conventional fatigue tests [19, 20]. As mentioned above, the maximum temperature of the beam window portion of the mercury target vessel reaches 250 °C. Therefore, this fatigue strength degradation by temperature is important for lifetime of the target vessel. The design curve of the JSNS target at 95% of failure probability [21] is plotted in Fig. 6. It is noted that the design curve was converted from ε_a–N_f relation to σ_a–N_f relation using a constant Young's modulus. It can be seen that the SA 316L tested in HT is below the design curve. Therefore is the target vessel would have the possibility to fail in gigacycle region, if the material would not be hardened by the proton and neutron irradiation.

3.2.3. Effect of mercury on fatigue strength

The S–N curves of as-received and 5000 hours mercury-immersed SA 316L tested in air at room temperature obtained by the ultrasonic fatigue tests are summarised in Fig. 7. The fatigue strength of mercury-immersed specimen in high-cycle region (from 10^4 to 10^7 cycles) seems to be lower than that of as-received specimen, based on the number of data available. The effect of mercury is seems to be relatively smaller than the effect of temperature. The slope of fatigue degradation, a, in Eq. (5) in mercury-immersed specimen is −8.78.

It was reported that a surface thin layer of less than 10 μm in thickness is slightly hardened by mercury immersion at 150 °C [22]. However, since the hardened layer is thin, it was not contributing to increase the fatigue strength as the cold worked specimen. On the other hand, it was reported that the fatigue strength is degraded by in mercury under conventional tensile and bending fatigue

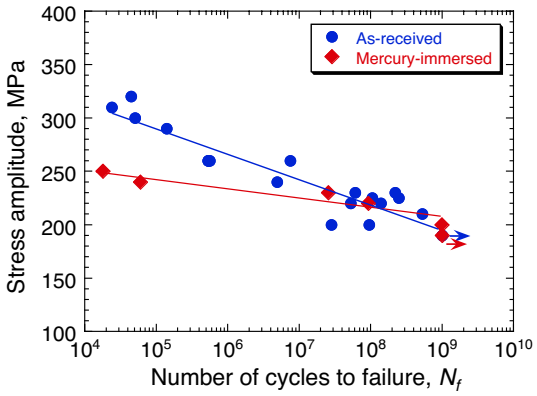

Fig. 7. *S*–*N* curves of as-received and mercury-immersed SA 316L tested in air at room temperature.

tests [11–13, 19], and experimental results seems to show the same trend with the previously reported results in mercury. However, it is noted that the mechanism of the degradation of fatigue strength in this experiment is different from the previous experiment. The former may caused by surface hardening by mercury immersion, the latter is caused by change of crack growth rate by mercury. Details will be discussed in future work.

3.3. Mechanical properties change by cyclic loading

3.3.1. Residual strength

Fig. 8 shows the relationship between the residual strength after fatigue test and the number of cycles for SA and 10%CW 316L at room temperature. It can be seen that the residual strength of SA 316L is increased with the number of cycles despite the fact the specimens have fatigue cracks. On the other hand, in the case of 10%CW 316L, the residual strength around 10^6 cycles is facing at the level of SA 316L. And at cycles higher than 10^7 cycles the residual strength seems

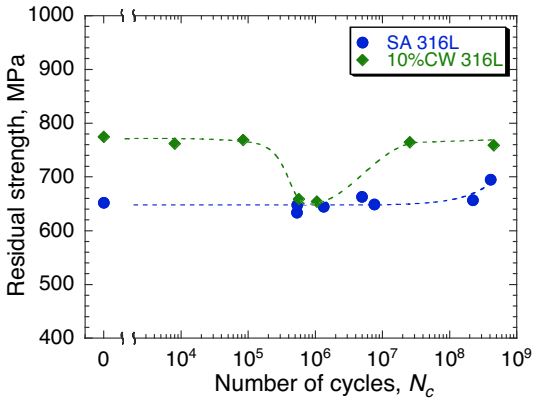

Fig. 8. Relationship between the residual strength and the number of cycles for SA and 10%CW 316L at room temperature.

to be recovered to the level of the non fatigued material.

3.3.2. Microhardness change by cyclic loading

Fig. 9 shows the change in the universal hardness as a function of the number of cycles at room temperature. It is noted that the universal hardness in each number of cycles is the average value of 5 data points. It is well known that the hardness is correlated with the tensile strength [23]. It can be seen in Fig. 9 that the hardness increases with the number of cycles in the case of SA 316L, and shows a similar trend with the residual strength (see Fig. 8). In the cases of 10%CW and 20%CW 316L, it can be seen that cyclic softening is observed at cycles below 10^6 cycles. On the other hand, above 10^6 cycles, cyclic hardening is seen for both the 10%CW and the 20%CW 316L. The rate of increase in hardness as a function of the number cycles above 10^6 cycles for 10%CW 316L is obviously larger than that of 20%CW 316L, and the hardness seems to saturate around 4.8 GPa.

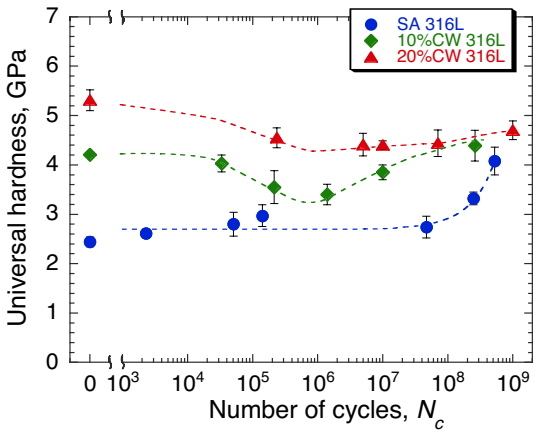

Fig. 9. Change in the hardness as a function of the number of cycles for SA, 10% CW, and 20% CW 316L tested in room temperature.

3.3.3. Fracture surface

Fig. 10 shows the typical example of the fracture surface of the as-received and fatigue-tested specimens for SA after the tensile tests. It can be seen that the reduction of area at necking is reduced by increasing the number of cycles. Reduction of area for (a) without cyclic loading, (b) N_f=7.51×10^6, and (c) N_f=2.21×10^8 are 15.2%, 25.0%, and 29.8%, respectively. It is suggested that the ductility is reduced by cyclic loading. Roughness around the edge part on the fracture surfaces of (b) and (c) are smoother than that of (a), because of the existence of cracks caused by the fatigue around the surface of the specimens (b) and (c).

3.4. Crack observation

The surface of fatigue tested specimens were observed using optical microscope and SEM. In the case of SA 316L, in most specimens, fatigue cracks were not observed from the observations of the surface because the cracks were closed

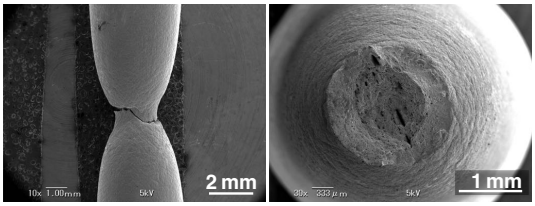

(a) W/O cyclic loading

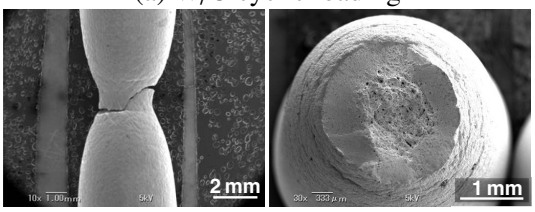

(b) σ_a=260 MPa N_f=7.51×10^6

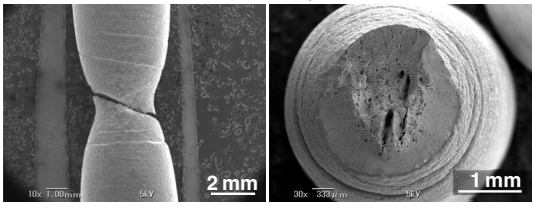

(c) σ_a=230 MPa N_f=2.21×10^8

Fig. 10. Typical examples of the fracture surfaces after tensile tests for SA 316L at room temperature obtained by SEM.

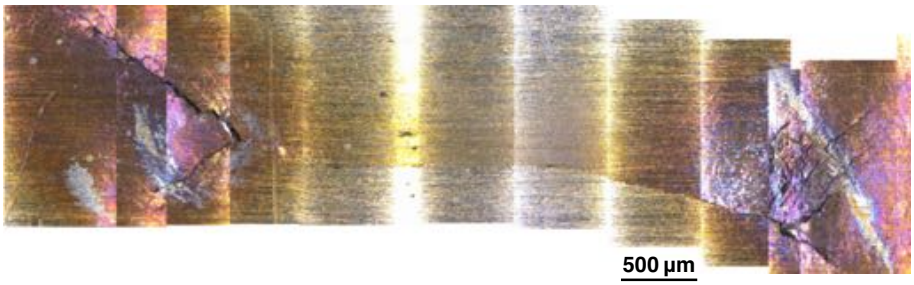

Fig. 11. Entire image of the surface crack of a 20%CW 316L specimen, obtained by optical microscopy.

and tiny. However, in the case of 20%CW 316L, the surface crack can be observed. Fig. 11 shows an example of the surface and cross sectional crack images of fatigue crack for 20%CW 316L tested at σ_a=435 MPa and N_f=7.20×10^8. It can be seen that the tempering color of the surface resulting from the temperature rising just before failure is recognized around the multiple small cracks. The main crack is propagating from the multiple crack and its direction is 45° of the loading direction. Fig. 12 shows the cross-sectional images of the crack for 20%CW 316L shown in Fig. 11, obtained by SEM. It can be seen that the small cracks are starting at the specimen surface and the main crack is also propagating from surface. In this experiment, internal failures originated by a fatigue crack propagating from an inclusion were not observed, regardless of cold work level.

4. Discussion

4.1. Temperature rise just before failure

In the ultrasonic fatigue test, the abrupt temperature rise just before failure was observed regardless of the testing temperature as shown in Fig. 4. Fig. 13

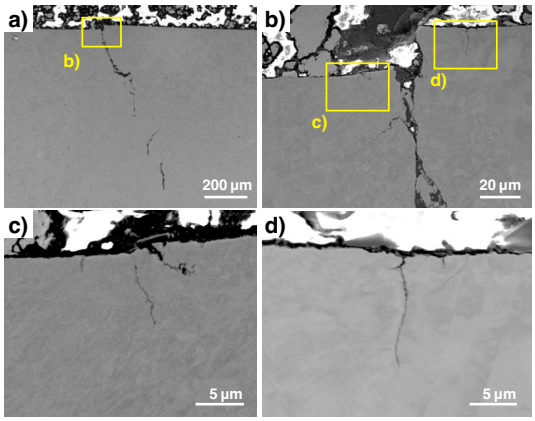

Fig. 12. Cross-sectional SEM images of fatigue failed specimen with multiple cracks.

shows the rescaled temperature histories just before failure for SA 316L tested at 260 MPa at room temperature. It is noted that the number of cycles is estimated from the equivalent frequency and saw-like temperature change is correlated with the timing of intermittent loading and arresting. It can be seen that the abruptly increase of surface temperature is recorded four times at around 7.34×10^6 and 7.38×10^6 cycles. These abrupt temperature rise might be related to the initiation and propagation of the fatigue cracks. In our experiment, the fatigue test was stopped when the resonance frequency was shifted by ±500 Hz from initial level by the fatigue crack. At this moment the maximum temperature just before failure seemed to be depending on the applied stress. This temperature rise is also reported for carbon steel and aluminium alloys, and it is suggested that the plastic deformation around the crack tip contributes to the temperature rise [24, 25]. It is proposed that the detection of the macro fatigue crack initiation of the structural material by measuring the temperature distribution could be done using thermog-

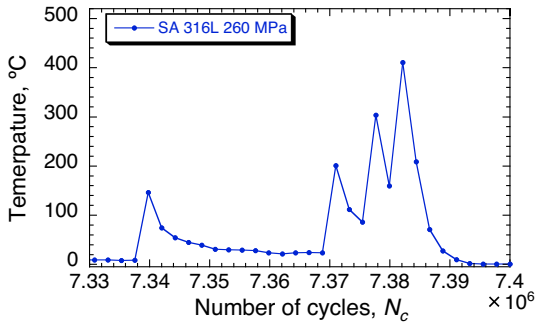

Fig. 13. Change in the specimen surface temperature just before failure as a function of the number of cycles.

raphy [26], and it is also proposed that the evaluation of the dissipated energy by measuring the temperature distribution could be used for estimating the fatigue limit [27]. Furthermore, these methods were performed under the conditions of conventional fatigues (~10 Hz), and seems to be applicable for our case regardless of strain rate. The residual strength of the fatigue-failed specimen, which contains the small and closed fatigue cracks, is hardly changed in comparison with the specimen without any fatigue damage. Therefore, the in situ measurement of the temperature distribution through the non-contact monitoring technique has the possibility to detect fatigue cracks for not only the mercury target vessel but also nuclear structural component.

4.2. Effect of strain rate and temperature on fatigue strength

As shown in Fig. 5, fatigue strength of the ultrasonic fatigue tests performed at strain rate of 10^2 s^{-1} is higher than that of the conventional fatigue tests performed about 10^{-1} s^{-1}. The similar trends are reported in 50CrMo4[28] and type 304L stainless steels [29]. It is well known that the yield stress and the ultimate

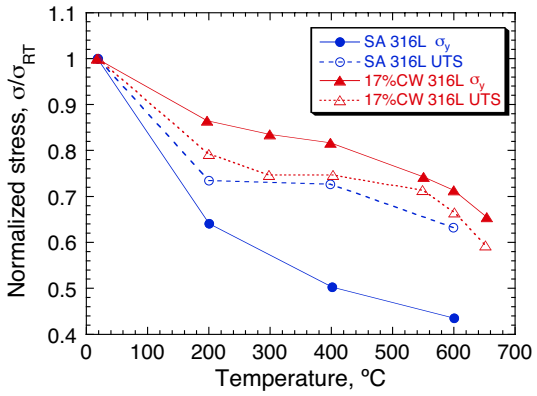

Fig. 14. Change in the normalized yield stress and ultimate tensile strength as a function of the temperature normalised at room temperature [32].

tensile strength (UTS) are varied by the temperature and the strain rate [30, 31]. Fig. 14 summarizes the change in the yield stress and the UTS as a function of the temperature for SA and 17%CW 316L [32]. It can be seen that the yield stress and the UTS are decreased with increasing in temperature. The reduction in the rate of yield stress and UTS of SA 316L from room temperer above to 250 °C seems to be larger than that of CW. Therefore the reduction of the fatigue strength by temperature for SA is slightly larger than that of CW, as shown before.

4.3. Cyclic hardening and softening

It is known that dynamic strain aging due to cyclic stress increases the hardness and the fatigue strength of the specimen [32–34]. For example, Hong et al., suggested that dynamic strain aging induces hardening and supresses crack initiation [32]. Kako et al., systematically investigated the occurrence of dynamic strain aging for SA by changing the temperature and the strain rate [34]. It was shown that in the case strain rates higher than 10^{-1}, the temperature range in which dy-

namic strain aging can occur is approximately 400~750 °C, that is, dynamic strain aging may not occur in our experimental condition.

As the other possible factor for cyclic hardening is the deformation-induced martensitic transformation. However, for type 316L stainless steel, it was reported that the martensitic transformation is not observed except for around fatigue crack by the cyclic-loading under room temperature, whereas observed in low temperature less than -100 °C [35]. It was also reported 316 SS dose not form deformation-induced martensite by the tensile testing up to 50% in engineering strain [36].

On the other hand, it is known that the dislocation density is increased by cold work level, and the hardness is proportional to the square root of the dislocation density [37]. Although the dislocation density of the specimen is not measured directly in this study, the cyclic hardening of SA seems to be caused by the accumulation of dislocation by cyclic loading. Fig. 15 shows the dislocation variation by cyclic loading as schematically. When the CW 316L is suffering cyclic load, the decreasing of the dislocation density caused by pre-existed dislocation due to the annihilation of pre-existed dislocation (D_a), and the rate of decreasing is higher than the rate of increase of the dislocation density by cyclic loading (D_c). Until the number of cycles reach up to a certain value (N'), since the decreasing of the pre-existed dislocation density, the decreasing by annihilation (D_a) and increasing by accumulation (D_c) of the dislocation density will reach up to a balance. Thereafter, the decreasing of the dislocation density due to the annihilation of pre-existed dislocation will be lower than the increment of the dislocation density caused by cyclic loading. In future work, we are planning to measure the dislocation density of the fatigue-tested specimens through the neutron diffraction

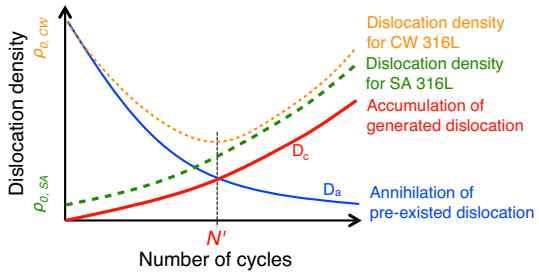

Fig. 15. Relationship between the dislocation density and the number of loading cycles.

method using the instrumentation of J-PARC.

In the case of the proton and neutron irradiation environment as for the mercury target vessel, accumulation of the dislocation due to displacement damage will occur during the operation. The cyclic softening, which took place in the cold-worked materials, will contribute to annihilate the radiation hardening by cyclic softening. It is known that hardness is well correlated with strength, e.g. yield stress, UTS, and fatigue strength [38]. Fig. 16 shows the schematic behavior of the overall hardness as a function of the time. In the initial stage of region *I*, hardness will increase with time due to the radiation hardening and cyclic hardening ($D_c > D_a$). In the next stage, region *II*, the hardness will gradually saturate, that is radiation and cyclic hardening will balance each other due to the cyclic softening ($D_c = D_a$). And in the final stage of region *III*, the hardness might be reduced by cyclic softening of pre-existing dislocation ($D_C < D_a$). This would result in annihilation of the radiation embrittlement and prolongation of the lifetime of the target vessel by cyclic softening.

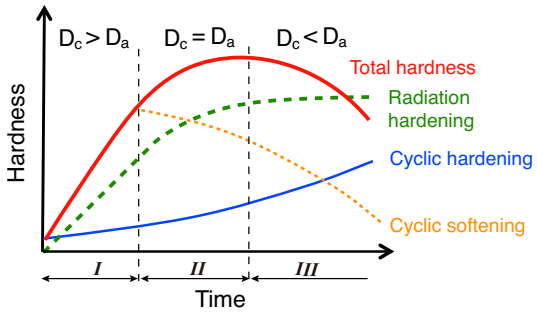

Fig. 16. Relationship between the hardness and time under the radiation environment.

5. Conclusion

Giga cycle fatigue behavior of type 316L stainless steel, which is the structural material of the mercury target vessel for the spallation neutron source, was investigated through the ultrasonic fatigue test under high-strain rate, at room temperature and 250 °C. The following was concluded:

(1) Fatigue strength in high-strain rate of around 10^2 s^{-1} is clearly higher than that found in conventional fatigues tests performed around 10^{-3}~10^{-1} s^{-1}. An obvious fatigue limit was not observed below 10^9 cycles, regardless of cold work level and testing temperature.

(2) Fatigue strength at 250 °C was obviously lower than at room temperature, regardless of cold work level. In the very high cycle region, fatigue data tested at 250 °C were below 316L the design curve of the JSNS target vessel. The reduction rate of the fatigue strength by temperature for SA is slightly higher than that of the CW 316L.

(3) Fatigue strength of mercury-immersed specimen up to 10^7 cycles seems to be lower than that of the as-received material, due to the mercury immersion.

(4) Apparent temperature rise was observed just before the failure of the ultrasonic fatigue test for both of SA and CW 316L specimens. This trend might be useful to detect the fatigue crack initiation of the components before failure, because the small induced fatigue crack did not lower the residual strength of the material.

(5) Cyclic dislocation hardening was responsible for the residual strength and hardness change of SA 316L. On the other hand, in the cases of 10%CW and 20%CW 316L, cyclic softening due to dislocation annihilation below 10^6 cycles and cyclic hardening appeared above 10^7 cycles.

Acknowledgements

This work was partly supported by the Japan Society for the Promotion of Science through the Grant-in-Aid for Scientific Research (Nos. 23360088 and 26820016).

References

[1] Japan Proton Accelerator Research Complex, http://j-parc.jp/index-e.html (2015).

[2] M. Futakawa, Material issues relating to high power spallation neutron sources, IOP Conf. Ser. Mater. Sci. Eng. 74 (2015) 012001–1–7.

[3] Material & Life Science Experimental Facility Construction Team, High intensity proton accelerator project (J-PARC) technical design report Material & Life science experimental Facility, Tech. rep., Japan Atomic Energy Agency, JAEA-Tech 2004-001 (2004).

[4] Z. Xiong, M. Futakawa, T. Naoe, K. Maekawa, Very high cycle fatigue in pulsed high power spallation neutron source, Adv. Mater. Res. 891–892 (2014) 536–541.

[5] M. Futakawa, T. Wakui, H. Kogawa, Y. Ikeda, Pressure wave issues in high power mercury target, Nucl. Inst. Meth. in Phys. Res. A 562 (2006) 676–679.

[6] D. A. McClintock, B. W. Riemer, P. D. Ferguson, A. J. Carroll, M. J. Dayton, Initial observations of cavitation-induced erosion of liquid metal spallation target vessels at the Spallation Neutron Source, J. Nucl. Mater. 431 (2012) 147–159.

[7] D. A. McClintock, B. J. Vevera, B. W. Riemer, F. X. Gallmeier, J. W. Hyres, P. D. Ferguson, Post-irradiation tensile properties of the first and second operational target modules at the Spallation Neutron Source, J. Nucl. Mater. 450 (2014) 130–140.

[8] S. X. Li, Effects of inclusions on very high cycle fatigue properties of high strength steels, Int. Mater. Rev. 57 (2012) 92—114.

[9] K. Takahashi, T. Ogawa, Evaluation of giga-cycle fatigue properties of austenitic stainless steels using ultrasonics fatigue test, J. Solid Mech. Mater. Eng. 2 (2008) 366–373.

[10] T. Ogawa, M. Nakane, K. Masaki, S. Hashimoto, Y. Ochi, K. Asano, Investigation of effect of pre-strain on very high-cycle fatigue strength of austenitic stainless steels, J. Power Energy Sys. 3 (2009) 38–50.

[11] J. P. Strizak, H. Tian, P. K. Liaw, L. K. Mansur, Fatigue properties of type 316LN stainless steel in air and mercury, J. Nucl. Mater. 343 (2005) 134–144.

[12] T. Naoe, Y. Yamaguchi, M. Futakawa, T. Wakui, Bending fatigue strength of austenitic stainless steel sus316 in mercury, J. Soci. Mater. Sci. Japan 59 (2010) 309–314.

[13] T. Naoe, Y. Yamaguchi, M. Futakawa, Quantification of fatigue crack propagation of an austenitic stainless steel in mercury embrittlement, J. Nucl. Mater. 431 (2012) 133–139.

[14] L. Medina-Almaz*á*n, T. Auger, D. Gorse, Liquid metal embrittlement of an austenitic 316l type and a ferritic-martensitic t91 type steel by mercury, J. Nucl. Mater. 376 (2008) 312–316.

[15] Y. Murakami (Ed.), Metal Fatigue: Effects of Small Defects and Nonmetallic Inculsions, Elsevier, 2002.

[16] K. Salama, R. K. Lamerand, The prediction of fatigue life using ultrasound testing, in: Ultrasonic Fatigue: Proceedings of the First International Conference on Fatigue and Corrosion Fatigue Up to Ultrasonic Frequencies, Metallurgical Society of AIME, New York, 1982, pp. 109–118.

[17] T. Naoe, M. Futakawa, A. Naito, H. Kogawa, Y. Ikea, Y. Motohashi, Evaluation of mechanical properties and microstructure in ion-irradiated surface layer, JSME Int. J. 48 (2005) 280–285.

[18] The Japan Society of Mechanical Engineers (Ed.), Standard Method of Statical Fatigue Testing, The Japan Society of Mechanical Engineers, 1981.

[19] H. Tian, P. K. Liaw, J. P. Strizak, L. K. Mansur, Effects of mercury on fatigue behavior of type 316 LN stainless steel: application in the spallation neutron source, J. Nucl. Mater. 318 (2003) 157–166.

[20] J. Huang, J. Yeh, S. Jeng, C. Chen, R. Kuo, High-cycle fatigue behavior of type 316l stainless steel, Mater. Trans. 47 (2006) 409–417.

[21] T. Wakui, M. Futakawa, H. Kogawa, S. Ishikura, Failure probability of multi-walled vessels for mercury target, J. Nucl. Sci. Technol. 44 (2007) 530–536.

[22] M. Futakawa, T. Wakui, H. Kogawa, H. Date, Mechanical property evaluation of nanoscale zone by indentation technique, in: Proceedings of JSME/ASME International Conference of on Materials and Processing 2002, The Japan Society of Mechanical Engineers, Japan, 2002, pp. 558–563.

[23] J. R. Chahoon, W. H. Broughton, A. R. Kutzak, The determination of yield strength from hardness measurements, Mater. Trans. 2 (1971) 1979–1983.

[24] N. Ranc, D. Wagner, P. C. Paris, Study of thermal effect associated with crack propagation during very high cycle fatigue tests, Acta Mater. 56 (2008) 4012–4021.

[25] D. Wagner, N. Ranc, C. Bathias, P. C. Paris, Fatigue crack initiation detection by an infrared thermography method, Fatigue Fract. Eng. Mater. Struct. 33 (2009) 12–21.

[26] T. Sakagami, T. Nishimura, S. Kubo, Y. Sakino, K. Ishino, Development of a self-reference lock-in thermography for remote nondestructive testing of fatigue crack (1st report, fundamental study using welded steel sample), Trans. JSME A72 (2006) 1860–1867.

[27] A. Akai, D. Shinozawa, T. Sakagami, Fatigue limit evaluation for austenitic stainless steel, J. Soc. Mater. Sci. Japan 61 (2012) 953–959.

[28] N. Schneider, B. Pyttel, C. Berger, M. Oechsner, Influence of frequency and testing technique on the fatigue behavior of quenched and tempered steel in the vhcf-regime, Adv. Mater. Res. 891–892 (2014) 1430–1435.

[29] T. Poulain, J. Mendez, G. Henaff, L. D. Baglion, Influence of the strain rate on the low cycle fatigue life of an austenitic stainless steel with a ground surface finish in different environments, Adv. Mater. Res. 891–892 (2014) 1320–1326.

[30] G. R. Johnson, W. H. Cook, A constitutive model and data for metals subjected to large strains, high strain rates and high temperatures, in: Proceedings of 7th International Symposium on Ballistics, International Ballistics Committee, Hague, Netherlands, 1983, pp. 541–547.

[31] K. Kawata, I. Miyamoto, M. Itabashi, On the effects of alloy components in the high velocity tensile properties, in: Proceedings of IMPACT ’87, Bremen, West Germany, 1987, pp. 349–356.

[32] S.-G. Hong, S. Yoon, S.-B. Lee, The effect of temperature on low-cycle fatigue behavior of prior cold worked 316l stainless steel, Int J. Fatigue 25 (2003) 1293–1300.

[33] S.-G. Hong, S.-B. Lee, Dynamic strain agin under tensile and lcf loading conditions, and their comparison in cold worked 316l stainless steel, J. Nucl. Mater 328 (2004) 232–242.

[34] K. Kako, Y. Miyahara, Y. Hide, M. Mayuzumi, Influence of the strain rate on the low cycle fatigue life of an austenitic stainless steel with a ground surface finish in different environments, J. Japan Inst. Metals 72 (2008) 206–210.

[35] J. Man, K. Obrlík, M. Petrenec, P. B. amd M. Smaga, A. Weidner, J. Dluhoš, T. Kruml, H. Biermann, D. Eifler, J. Polák, Stability of austenitic 316l steel against martensite formation during cyclic straining, Prodedia Eng. 10 (2011) 1279–1284.

[36] S. K. Varma, J. Kalyanam, L. E. Murr, V. Srinivas, Effect of grain size on deformation-induced martensite formation in 304 and 316 stainless steels during room temperature tensile testing, J. Mater. Sci. Lett. 13 (1994) 107–111.

[37] S. Takaki, T. Tsuchiyama, K. Nakashima, H. Hidaka, K. Kawasaki, Y. Futamura, Microstructure development of steel during severe plastic deformation, Metals Mater. Int. 10 (2004) 533–539.

[38] A. Casagrande, G. P. Cammarota, L. Micele, Relationship between fatigue limit and vickers hardness in steels, Mater. Sci. Eng. A 528 (2011) 3468–3473.